Proceedings of the ASME 2016 International Design Engineering Technical Conferences and Computers and Information in Engineering Conference
IDETC/CIE 2016
August 21-24, 2016, Charlotte, North Carolina

DETC2016-60349

NUMERICAL INVESTIGATIONS OF PARAMETRICALLY EXCITED NON-LINEAR MULTI DEGREE OF FREEDOM MICRO-ELECTROMECHANICAL SYSTEMS

Till J. Kniffka
Horst Ecker*
Institute of Mechanics and Mechatronics
TU Wien
1060 Vienna, Austria
Email: till.kniffka@tuwien.ac.at
Email: horst.ecker@tuwien.ac.at

Brian R. Mace
Roger Halkyard
Department of Mechanical Engineering
University of Auckland
Auckland 1010, New Zealand

ABSTRACT

More and more systems exploit parametric excitation (PE) to improve their performance compared to conventional system. Especially in the field of micro-electromechanical systems (MEMS) such technologies rapidly gain in importance. Different to conventional resonance cases PE may destabilise the system's rest position when parametrically excited time-periodically with a certain PE frequency. At such parametric resonances vibrations are only limited due to non-linearities. The system is repelled by the unstable rest position and enters a bifurcated limit cycle.

Finding these limit cycles has become more easy in recent years. Advances have been made in numerical path following tools regarding both their power and their user friendliness. As a result, designing such systems has become more common. Indeed, the focus of studies has been on 1DOF systems mostly.

However, for multi degree of freedom systems choosing a meaningful phase space to discuss the results is a task on its own. Quasi-modally transforming the equations of motion, the vibrations are decomposed allowing one to focus on the predominant modes. By concentrating on these predominant modes, continuation results can be displayed in meaningfully reduced phase-parameter spaces. Basins of attraction can be found in Poincaré sections of these phase-parameter spaces.

Employing these approaches, it is demonstrated how to investigate a non-linear 2DOF PE MEMS, how to change the characteristics of the limit cycles and how this affects their basins of attraction.

NOMENCLATURE

$\dot{(\,)} = \frac{\mathrm{d}}{\mathrm{d}t}$	time derivative
c_i	damping
k_i	stiffness
m_i	mass
x_i	displacement
z_i	modal displacement
ρ_i	Floquet multiplier
φ_i	eigenmode
ψ_i	phase shift
ω_i	natural angular frequency
Ω_{PE}	frequency of parametric excitation (PE-frequency)

*Address all correspondence to this author.

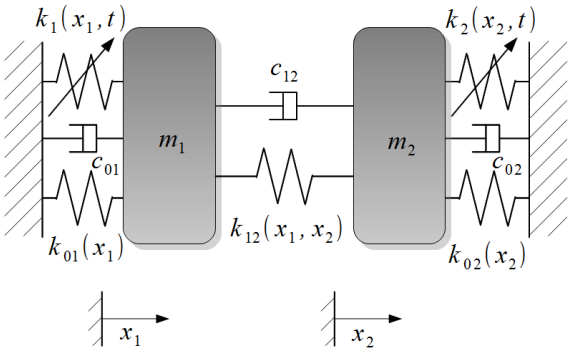

FIGURE 1. 2DOF LUMPED MASS MODEL FROM [4]. PE BY THE TIME-PERIODIC STIFFNESS CONSTANTS $k_{1/2}(x_{1/2},t)$.

INTRODUCTION

A vast number of publications exists on the dynamics of externally exited and self-exited non-linear systems. Far less research has been conducted for non-linear *parametrically excited* (PE) systems. Yet, for one degree of freedom (1DOF) non-linear PE systems progress has been made in recent years in understanding their behaviour and hence in the systems' performance [1–3]. Multi degree of freedom (MDOF) PE systems however have a larger set of differential equations and thus a larger number of parameters. Also, investigating such systems tends to be complex because of their multidimensional phase spaces.

Advances have been made in investigating such systems analytically [5]. This paper demonstrates some approaches to investigating multi degree of freedom non-linear PE systems numerically.

The parameter set employed (see Tab. 1) clearly refers to a micro system. The research leading to the presented results was motivated by a combdriven MEMS investigated by WELTE ET AL. [4]. The system in [4] is an extension to 2DOF of a 1DOF system introduced in [2]. In [2] a flexible mounted mass is parametrically excited by a periodically changing voltage fed into a comb shaped capacitor. The parametric resonances (PRs) are exploited as bandpasses for filtering electrical signals (see [2] for details). Other applications which can be modelled as illustrated in the next section include extension to 2DOF of 1DOF systems such as MEMS energy harvesters [3] or MEMS mass sensors [6]. PE has proven to be beneficial for designing MEMS systems in order to outperform conventional design in terms of efficiency and performance. The numerical studies presented are motivated by MEMS and mainly refer to the dynamics of MEMS. However, the normalisation of the equations leads to very general and dimensionless expressions, which are not limited to MEMS.

After introducing a lumped mass model for a 2DOF non-linear (PE) MEMS the basic effects of PE are explained and demonstrated. The model's behaviour at PRs is investigated numerically employing the MATLAB-based package MATCONT [7] for numerical continuation. Limit cycles and their stability are examined. Their basins of attraction are determined both by a time integration and an iterative method. All results are displayed in *quasi-modally* transformed and reduced phase spaces and Poincaré sections of those. The quasi-modal transformation is explained in detail in the fourth section.

TABLE 1. SYSTEM PARAMETERS (TAKEN FROM [5]).

Parameter	Symbol	Value	Unit
Mass	m_1	$1.22 \cdot 10^{-10}$	kg
	m_2	$2.44 \cdot 10^{-10}$	kg
Damping	c_{01}	$1.94 \cdot 10^{-8}$	$\mathrm{N\,m^{-1}\,s}$
	c_{12}	$0.97 \cdot 10^{-8}$	$\mathrm{N\,m^{-1}\,s}$
	c_{12}	$1.94 \cdot 10^{-8}$	$\mathrm{N\,m^{-1}\,s}$
Linear Stiffness	$k_{01,\mathrm{lin}}$	3.505	$\mathrm{N\,m^{-1}}$
	$k_{12,\mathrm{lin}}$	1.753	$\mathrm{N\,m^{-1}}$
	$k_{02,\mathrm{lin}}$	3.505	$\mathrm{N\,m^{-1}}$
Non-linear Stiffness	$k_{01,\mathrm{nlin}}$	$18 \cdot 10^9$	$\mathrm{N\,m^{-3}}$
	$k_{12,\mathrm{nlin}}$	$9 \cdot 10^9$	$\mathrm{N\,m^{-3}}$
	$k_{02,\mathrm{nlin}}$	$18 \cdot 10^9$	$\mathrm{N\,m^{-3}}$
Linear PE Stiffness	$k_{\mathrm{PE},1,\mathrm{lin}}$	0.2281	$\mathrm{N\,m^{-1}}$
	$k_{\mathrm{PE},2,\mathrm{lin}}$	0.2281	$\mathrm{N\,m^{-1}}$
Non-linear PE Stiffness	$k_{\mathrm{PE},1,\mathrm{nlin}}$	$-1.056 \cdot 10^{10}$	$\mathrm{N\,m^{-3}}$
	$k_{\mathrm{PE},2,\mathrm{nlin}}$	$-1.056 \cdot 10^{10}$	$\mathrm{N\,m^{-3}}$
Nat. Ang. Frequencies	ω_1	136280	$\mathrm{s^{-1}}$
	ω_2	221090	$\mathrm{s^{-1}}$

MODELLING

The approaches presented in the following generally hold for any PE non-linear MDOF system. However for simplicity only a 2DOF system is considered. This 2DOF MEMS is modelled by a lumped mass model according to Fig. 1 [4]. Two rigid bodies with masses m_1 and m_2 are linked to each other and their environment by non-linear springs with stiffness parameters $k_{ij}(x_i,x_j) = k_{ij,\mathrm{lin}} + k_{ij,\mathrm{nlin}}(x_i - x_j)^2$ and viscoelastic dampers with damping constants c_{ij}. In addition, both bodies are coupled to the inertial frame with non-linear springs with time-periodic

stiffness functions

$$k_i(x_i,t) = k_{\mathrm{PE},i}(x_i)(1+\cos(\Omega_{\mathrm{PE}}t)), \tag{1a}$$

$$k_{\mathrm{PE},i}(x_i) = k_{\mathrm{PE},i,\mathrm{lin}} + k_{\mathrm{PE},i,\mathrm{nlin}}x_i^2. \tag{1b}$$

The system is not excited by external forces, but by this PE via the time-periodic stiffness constants. The parameter values are listed in Tab. 1. The governing equation of motion can be written as

$$\mathbf{M}\ddot{\mathbf{x}} + \mathbf{C}\dot{\mathbf{x}} + \mathbf{K}(\mathbf{x})\mathbf{x} + \mathbf{K}_{\mathrm{PE}}(\mathbf{x})\cos(\Omega_{\mathrm{PE}}t)\mathbf{x} = \mathbf{0}, \tag{2}$$

with $\mathbf{M} = \mathrm{diag}(m_i)$ and $\mathbf{K}_{\mathrm{PE}} = \mathrm{diag}(k_{\mathrm{PE},i,\mathrm{lin}} + k_{\mathrm{PE},i,\mathrm{nlin}}x_i^2)$. The stiffness matrix $\mathbf{K}(\mathbf{x})$ and the damping matrix $\mathbf{C}$ are fully occupied.

Some PE MEMS have PE mechanisms which have to be modelled as stated in Eq. (1a). Examples for such systems are combdriven MEMS [2, 6]. Using other PE mechanisms, such as mechanical PE (see [3] for example), the offset of the fluctuation of the PE stiffness may vanish, i.e.

$$k_i(x_i,t) = k_{\mathrm{PE},i}(x_i)(\cos(\Omega_{\mathrm{PE}}t)). \tag{3}$$

Modelling PE according to Eq. (3), the natural frequencies of the corresponding linear non-PE system and the system's qualitative behaviour at PRs are not affected by the PE stiffness parameter $k_i(x_i,t)$. Modelling according to Eq. (1a), the linear PE stiffness constants $k_{\mathrm{PE},i,\mathrm{lin}}$ have an impact on the system's natural frequencies, while the non-linear PE stiffness constants $k_{\mathrm{PE},i,\mathrm{nlin}}$ determine the qualitative behaviour of the bifurcating limit cycles and hence on the amplitudes and the phase shifts of the vibrations at PRs [2, 5].

EFFECTS OF PARAMETRIC EXCITATION

The stability of time-periodic systems cannot be analysed by investigating the Jacobian of the equations of motion, since this matrix is time-variant. Instead the Monodromy matrix is evaluated. This maps a set of fundamental states of the system to another one after a certain period. Obviously, the period of the vibrations ensures such a mapping of a set of fundamental states (see for example [8]). But the period of the PE also fulfils this criterion [9]. Employing the period of the PE often is more convenient, since it is known.

In either case, the real parts of the eigenvalues of the Monodromy matrix give information about the state's stability. These *characteristic multipliers* ρ are sometimes also named *Floquet multipliers* referring to the French mathematician A.M.G. Floquet. Values of $\max(\Re\{|\rho|\}) < 1$ indicate stable states. However, if the PE period is used for the mapping, the Floquet multipliers ρ for different PE frequencies can be compared to each other qualitatively only after normalising them to the PE period [10].

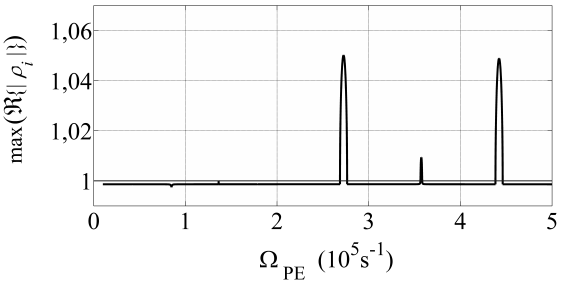

FIGURE 2. MAXIMUM OF THE REAL PARTS OF THE FLOQUET MULTIPLIERS DEPENDING ON THE PE FREQUENCY. $\max\Re\{|\rho|\} > 1$ INDICATES UNSTABLE STATES.

Investigating the Floquet multipliers of the rest position of the system introduced above leads to Fig. 2. Note, that in contrast to other references, here the Floquet multipliers ρ are normalised with respect to the PE period to ensure comparability for different PE frequencies. Three instability intervals of the rest position can be identified: $\Omega_{\mathrm{PE}} = 2\omega_1; \omega_1+\omega_2; 2\omega_2$. Depending on the damping being present, the rest position of PE system may be unstable at so called *parametric resonances* (PRs), i.e.

$$\Omega_{\mathrm{PR},i,n} = \frac{2\omega_i}{n}, \quad \forall\, n \in \mathbb{N}, \tag{4}$$

where ω_i are the undamped natural angular frequencies of the corresponding linear non-PE system. For the parameters in Tab. 1 the damping suppresses all but two PRs: $\Omega_{\mathrm{PR},1,1} = 2\omega_1 = 272560\,\mathrm{s}^{-1}$ and $\Omega_{\mathrm{PR},2,1} = 2\omega_2 = 442180\,\mathrm{s}^{-1}$. These PRs can be recognised as the two large peaks in Fig. 2. Time series at both PRs are presented in Fig. 3a and b. At both PRs the system is repelled by the destabilised rest position starting with an initial disturbance $\mathbf{x} = [10^{-15}, 10^{-15}, 0, 0]^{\mathrm{T}}$. It is attracted by stable limit cycles which are approached with overshooting oscillating amplitudes.

If the system has more than one degree of freedom, also *parametric combination resonances* (PCRs) may occur, e.g.

$$\Omega_{\mathrm{PCR},ij,n} = \frac{\omega_i + \omega_j}{n}, \quad \forall\, n \in \mathbb{N}. \tag{5}$$

In Fig. 2 one PCR manifests: $\Omega_{\mathrm{PR},12,1} = \omega_1 + \omega_2 = 357370\,\mathrm{s}^{-1}$. A time series is given in Fig. 3c. The vibration amplitudes are similar to the ones of the vibrations at the PRs, but the limit cycles are approached slowly. Note, that this behaviour can also be

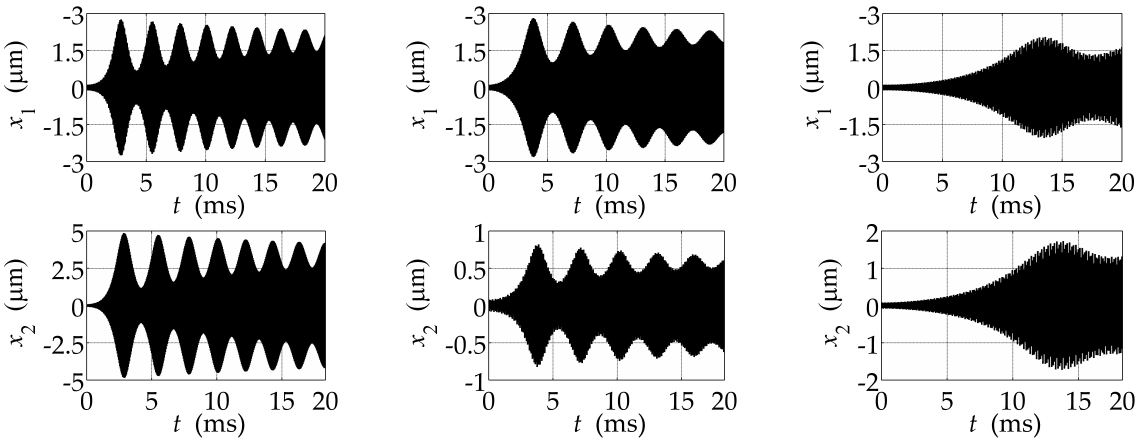

(a) $\Omega_{\mathrm{PE}} = 2\omega_1$ (b) $\Omega_{\mathrm{PE}} = 2\omega_2$ (c) $\Omega_{\mathrm{PE}} = \omega_1 + \omega_2$

FIGURE 3. TIME SERIES AT THE PARAMETRIC RESONANCES $\Omega_{\mathrm{PR}} = 2\omega_1; 2\omega_2$ AND AT THE PARAMETRIC COMBINATION RESONANCES $\Omega_{\mathrm{PCR}} = \omega_1 + 2\omega_2$.

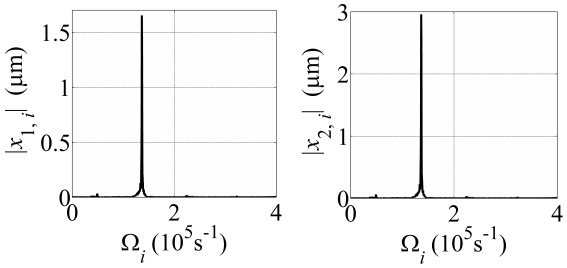

FIGURE 4. FFTS OF THE LIMIT CYCLE VIBRATIONS AT THE PR $\Omega_{\mathrm{PR},1} = 2\omega_1$.

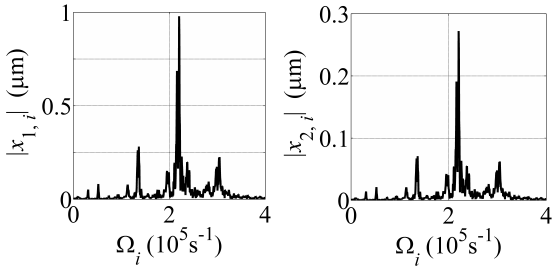

FIGURE 5. FFTS OF THE LIMIT CYCLE VIBRATIONS AT THE PR $\Omega_{\mathrm{PR},2} = 2\omega_2$.

seen from Fig. 2 since the slope of the envelope at $t = 0$ is given by $\max(\Re\{|\rho|\})\Big|_{\Omega_{\mathrm{PE}}}$.

In addition to PCRs, for multi degree of freedom systems also *parametric anti-resonances* (PARs) exist at the PE frequencies

$$\Omega_{\mathrm{PAR},ij,n} = \frac{|\omega_i - \omega_j|}{n}, \quad \forall\, n \in \mathbb{N}, \tag{6}$$

if damping is present. Different to the destabilising effects of PRs and PCRs, such intervals are associated with the interesting effect of enhanced energy dissipation which was first discovered by Tondl [11]. Energy is transferred periodically between both involved modes i and j making use of the higher modal damping of the higher mode more efficiently [12]. For the parameters in Tab. 1 one PAR exists at $\Omega_{\mathrm{PE}} = \omega_2 - \omega_1 = 84810\,\mathrm{s}^{-1}$. It is visible in Fig. 2 as a tiny notch.

Analysing the vibrations at the PRs in the frequency domain reveals that at each PR $\Omega_{\mathrm{PR},i,n} = \frac{2\omega_i}{n}$ primarily the mode i is excited (see Fig. 4,5, see [13] for example, too). Thus for both displacements $x_1(t)$ and $x_2(t)$ the frequency spectra qualitatively are the same, being dominated by a peak at this frequency. Only one mode produces significant amplitudes in the motions of the bodies. This mode's vibration is scaled to the physical displacements x_k by the kth entry of each mode's eigenvector. Also, for PCRs $\Omega_{\mathrm{PCR},ij,n} = \frac{\omega_i + \omega_j}{n}$ both corresponding modes i and j are excited (see [13] for example).

QUASI-MODAL TRANSFORMATION

Linearising at the rest position and setting $\mathbf{K}_{\mathrm{PE}} = \mathbf{0}$ describes a linear, time-invariant (LTI) system for which the system's undamped natural angular frequencies ω_i and the corresponding

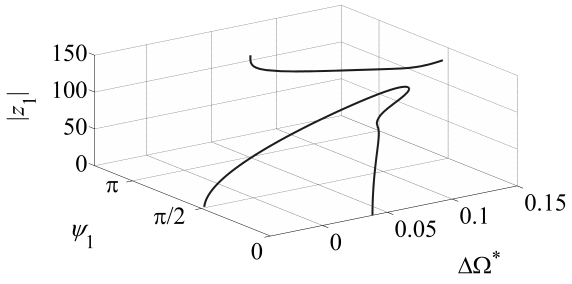

FIGURE 6. BIFURCATED LIMIT CYCLES AT THE PR $\Omega_{\mathrm{PR},1} = 2\omega_1$. AMPLITUDE z_1 AND PHASE SHIFT ψ_1 OF THE FIRST MODE DEPENDING ON THE DETUNING $\Delta\Omega^* = (\Omega_{\mathrm{PE}} - \Omega_{\mathrm{PR},1})10^{-5}$s OF THE PE FREQUENCY Ω_{PE}.

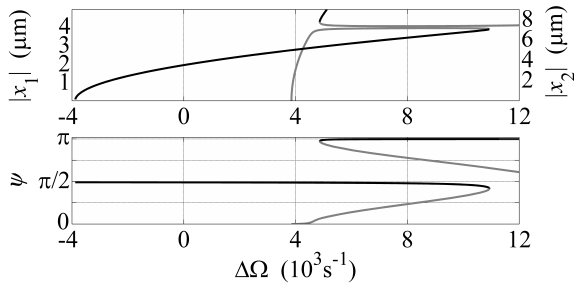

FIGURE 7. BIFURCATED LIMIT CYCLES AT THE PR $\Omega_{\mathrm{PR},1} = 2\omega_1$. AMPLITUDES AND PHASE SHIFTS OF THE PHYSICAL DISPLACEMENTS x_1 AND x_2 DEPENDING ON THE DETUNING $\Delta\Omega = \Omega_{\mathrm{PE}} - \Omega_{\mathrm{PR},1}$ OF THE PE FREQUENCY Ω_{PE}.

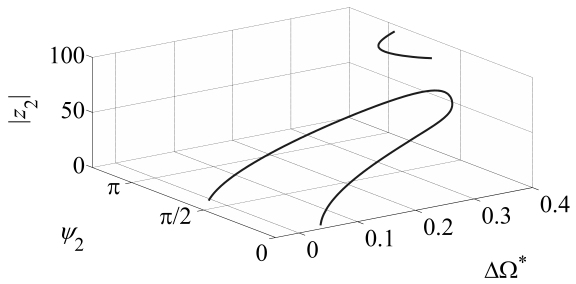

FIGURE 8. BIFURCATED LIMIT CYCLES AT THE PR $\Omega_{\mathrm{PR},2} = 2\omega_2$. AMPLITUDE z_2 AND PHASE SHIFT ψ_2 OF THE SECOND MODE DEPENDING ON THE DETUNING $\Delta\Omega^* = (\Omega_{\mathrm{PE}} - \Omega_{\mathrm{PR},2})10^{-5}$s OF THE PE FREQUENCY Ω_{PE}.

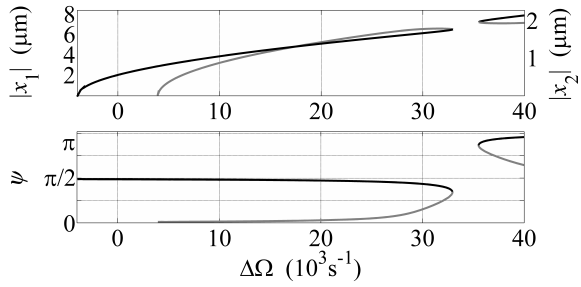

FIGURE 9. BIFURCATED LIMIT CYCLES AT THE PR $\Omega_{\mathrm{PR},2} = 2\omega_2$. AMPLITUDES AND PHASE SHIFTS OF THE PHYSICAL DISPLACEMENTS x_1 AND x_2 DEPENDING ON THE DETUNING $\Delta\Omega = \Omega_{\mathrm{PE}} - \Omega_{\mathrm{PR},2}$ OF THE PE FREQUENCY Ω_{PE}.

eigenmodes φ_i can be computed. These modes can be mass normalised and combined in the modal matrix $\phi = [\varphi_1\ \varphi_2\ ...\ \varphi_n]$. Employing this modal matrix ϕ, the displacement vector $\mathbf{x}$ can be transformed to the modal displacements $\mathbf{z}$ by

$$\mathbf{x} = x^* \phi \mathbf{z}. \tag{7}$$

Introducing a scaling parameter x^* leads to dimensionless quasi-modal displacements $\mathbf{z}$ as well as a sufficient scaling for evaluating the differential equations numerically. Such a transformation decouples the set of differential equations of a LTI system.

If $\mathbf{K}_{\mathrm{PE}} \neq \mathbf{0}$ or if $\mathbf{K} = \mathbf{K}(\mathbf{x})$, Eq. (2) is not decoupled by such a transformation. In this case, as explained in the previous section, the eigenvalue problem is time dependent. Hence φ_i are not its eigenmodes and z_i are not its modal displacements. This becomes clear in Fig. 5: both displacements x_1 and x_2 cannot be described exactly just by harmonics with the angular frequencies ω_1 and ω_2. Such eigenmodes, natural frequencies and modal displacements cannot be calculated for time-variant systems. Yet, the vibrations at PRs can be approximated satisfactorily by a superposition of φ_i with amplitudes z_i, as indicated by the dominance of the regarding modes in the spectra (see Fig. 4,5). Thus, for PE systems, φ_i are called *quasi-modes* and z_i *quasi-modal* displacements [10]. The next section demonstrates the high accuracy of this approximation by comparing the amplitudes of both modes along the bifurcated limit cycles at PRs.

BIFURCATION ANALYSIS AT PARAMETRIC RESONANCES

Employing a path-following software a numerical continuation of the solutions of Eq. (2) could be performed to study the system's behaviour. Indeed, displaying and analysing the results in the five dimensional parameter phase space (Ω_{PE}-$|x_1|$-$|x_2|$-ψ_1-ψ_2, e.g.) would be challenging. However, as it was shown in the previous sections, only one mode is predominantly excited at PR and this mode can be investigated by the quasi-modal decomposition. This allows one to focus on the important parameters of the transformed phase space.

In Fig. 6 the first bifurcated limit cycles at the PR $\Omega_{\mathrm{PR},1} = 2\omega_1$ are shown in the quasi-modally reduced parameter phase space $\Delta\Omega^*$-ψ_1-$|z_1|$. Here $|z_1|$ is the first mode's amplitude and ψ_1 its phase shift. The detuning of the PE frequency Ω_{PE} is denoted with $\Delta\Omega^* = (\Omega_{\mathrm{PE}} - \Omega_{\mathrm{PR},1})10^{-5}\mathrm{s}$. The centre of the PR $\Omega_{\mathrm{PE}} = 272560\,\mathrm{s}^{-1}$ is indicated by $\Delta\Omega^* = 0$. Displaying the second mode's amplitude in Fig. 10a agrees with the frequency spectra (Fig. 4) of the vibrations at this PR. The second mode's amplitudes are comparatively small compared to those of the first mode. This means that all the important information about the behaviour of the system at the PR can be given in Fig. 6 in the quasi-modally reduced parameter phase space.

The results of the transformation of this modal coordinates back to the physical ones employing Eq. (7) is depicted in Fig. 7. The approximations of both displacements have identical functional behaviour on different scales: Eq. (7) expresses that

$$x_k = x^* \sum_{l=1}^{n} \varphi_{lk} z_l \approx x^* \varphi_{ik} z_i,\ k = 1,2 \tag{8}$$

because $\varphi_{lk}\big|_{l\neq i} \ll \varphi_{ik}$ holds. Hence the ratio of the masses' amplitudes is the ratio $x_1/x_2 = \varphi_{11}/\varphi_{12}$ of the entries of the first eigenmode to a very good approximation. Both displacements have the same phase shift ψ to the PE at the first PR. They are in opposite at the second PR, with $\psi_1 = \psi$ and $\psi_2 = -\psi$.

The amplitude $|x_1|$ of displacement of the first mass can be read from the left-hand side of the amplitude characteristic Fig. 7, while the amplitude $|x_2|$ of the displacement of the second mass is denoted at the right-hand side.

Not all limit cycles depicted in Figs. 6 and 7 are stable. Unstable limit cycles are indicated grey in Fig. 7. At the centre frequency $\Omega_{\mathrm{PE}} = 272560\,\mathrm{s}^{-1}$ ($\Delta\Omega = 0$) only one state is stable: $[x_1,\ x_2]^{\mathrm{T}} = [1.91,\ 3.50]^{\mathrm{T}}\,\mathrm{nm}$. Within the presented frequency interval at most three states are stable. At the right hand side of the second bifurcation point $\Delta\Omega = 3853\,\mathrm{s}^{-1}$ two stable limit cycles may occur in addition to the stable rest position $x_1 = x_2 = 0$.

Similar results are obtained for the PR $\Omega_{\mathrm{PR},2} = 2\omega_2$. In Fig. 8 the first bifurcated limit cycles are displayed in the quasi-modally reduced parameter phase space $\Delta\Omega^*$-ψ_2-$|z_2|$, with $|z_2|$ the second mode's amplitude and ψ_2 its phase shift. The detuning of the PE frequency Ω_{PE} is denoted with $\Delta\Omega^* = (\Omega_{\mathrm{PE}} - \Omega_{\mathrm{PR},2})10^{-5}\mathrm{s}$. $\Delta\Omega^* = 0$ marks the centre of the PR $\Omega_{\mathrm{PE}} = 442180\,\mathrm{s}^{-1}$. The same as for the PR $\Omega_{\mathrm{PR},1} = 2\omega_1$, the continuation results of the first mode's amplitude in Fig. 10b agrees with the FFTs (Fig. 5) of the vibrations at the PR $\Omega_{\mathrm{PR},2} = 2\omega_2$. The first mode's amplitude is comparably small to that of the second mode. By analogy to the previously discussed PR, again all important information about the behaviour of the system at the PR can be given in Fig. 8 in the quasi-modally reduced parameter phase space.

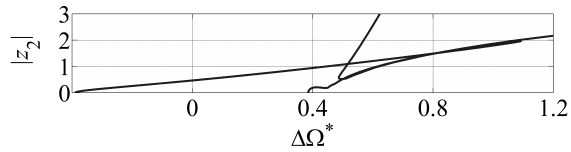

(a) $\Omega_{\mathrm{PE}} = \Omega_{\mathrm{PR},1} = 2\omega_1$

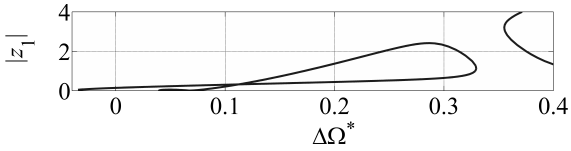

(b) $\Omega_{\mathrm{PE}} = \Omega_{\mathrm{PR},2} = 2\omega_2$

FIGURE 10. AMPLITUDES OF THE LESS EXCITED MODES ALONG THE BIFURCATED LIMIT CYCLES. THE DETUNING $\Delta\Omega = \Omega_{\mathrm{PE}} - \Omega_{\mathrm{PR,i}}$ OF THE PE FREQUENCY Ω_{PE}.

The same as for the previous PR, the transformation of these modal coordinates back to the physical ones is depicted in Fig. 9. The amplitude $|x_1|$ of displacement of the first mass can be read from the left-hand side of the amplitude characteristic, while the amplitude $|x_2|$ of the displacement of the second mass is denoted at the right-hand side. Both displacements have the same phase shift ψ to the PE. For this PR the ratio of the masses' amplitudes is the ratio of the entries of the second mode, i.e. $x_1/x_2 = \varphi_{21}/\varphi_{22}$.

As for the first PR, not all limit cycles depicted in Fig. 8,9 are stable. Unstable Limit cycles are indicated grey in Fig. 9. At the centre frequency $\Omega_{\mathrm{PE}} = 442180\,\mathrm{s}^{-1}$ only one state is stable: $[x_1,\ x_2]^{\mathrm{T}} = [2.07,\ 0.56]^{\mathrm{T}}\,\mathrm{nm}$. Different to the first PR, within the presented frequency interval here at maximum two states are stable. At the right hand side of the second bifurcation point $\Delta\Omega = 3923\,\mathrm{s}^{-1}$ one stable limit cycle may occur in addition to the stable rest position $x_1 = x_2 = 0$.

As illustrated in Figs. 7 and 9 the rest position is unstable/stable accordingly to whether the bifurcating limit cycle is stable/unstable. Also, averaging and linearising Eq. (2) leads to a Jacobian with eigenvalues $\lambda = 0$ of multiplicity 2 at the bifurcation points [5]. The bifurcations thus have the characteristic of saddle-node bifurcations with the unstable solution as the repelling saddle and the stable one as the attracting node [14]. As the angular frequency of the limit cycles is $\omega_i = 1/2\ \Omega_{\mathrm{PR,i}}$, the bifurcations also have a periodic doubling characteristic.

POINCARÉ MAPS AND BASINS OF ATTRACTION

Having found coexisting stable states the question arises, to which stable state the system is attracted starting from a certain state in the phase space. A first answer to this question can be given by investigating Poincaré maps. Here these maps are sectional planes for certain values of the angular PE frequency of

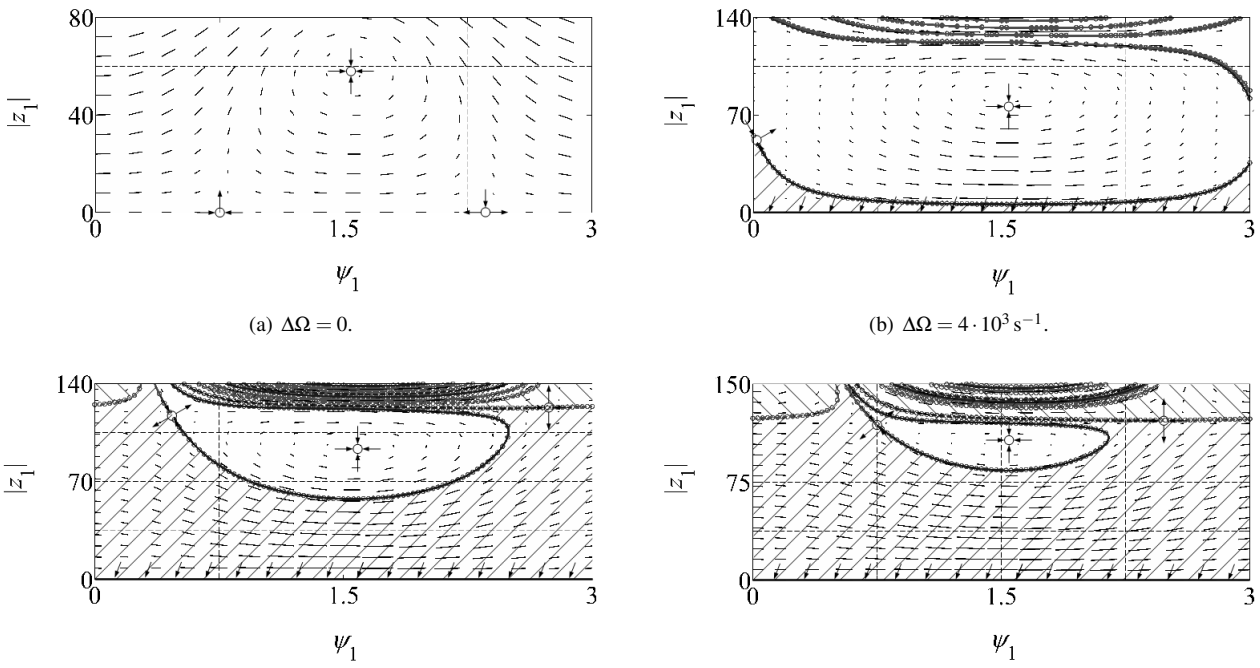

(a) $\Delta\Omega = 0$.

(b) $\Delta\Omega = 4 \cdot 10^3\,\mathrm{s}^{-1}$.

(c) $\Delta\Omega = 6 \cdot 10^3\,\mathrm{s}^{-1}$.

(d) $\Delta\Omega = 8 \cdot 10^3\,\mathrm{s}^{-1}$.

FIGURE 11. POINCARÉ MAPS AT THE PR $\Omega_{\mathrm{PR},1} = 2\omega_1$. HATCHED: BASIN OF ATTRACTION OF THE REST POSITION.

the quasi-modally reduced parameter phase spaces. This means that for a fixed Ω_{PE} the phase space is observed periodically at $t = k\frac{2\pi}{\omega_i}$. These maps can be derived numerically by iteration over the initial conditions and integration of $\mathbf{z}(t)$ over one period of $z_i(t)$. Here i indicates the dominant mode at a certain PR. The differences between the initial conditions and the final values are depicted as lines in Figs. 11 and 12.

However, without displaying the borders of the basins of attraction of each stable attractor, the Poincaré maps provide little understanding of the system's behaviour. These basins of attraction can be computed by scanning the phase space. Starting from any state, after a sufficient time the system will approach a stable state which can be identified by numerical integration. Indeed, such scanning means a high computational effort. Also, adapting the scanning resolution to the slope of the border between the basins of attraction is challenging. Without a well controlled scanning grid the accuracy will be unnecessary high at some parts of the Poincaré map and insufficiently low in other parts.

A more sophisticated approach is to take advantage of the repelling character of the saddles. Starting from a state near a saddle point the system is repelled and will approach a stable node over time. This means integrating backwards in time, the system's state will converge to the border of the adjacent basins of attraction. Since the system is repelled by this border, the system's state will never cross the border integrating backwards in time, but approach it asymptotically. For displaying the results in the Poincaré maps it is necessary to integrate numerically with a fixed time step which is an integral multiple of the period of $z_i(t)$. This demands an adjusted step control.

The results of both approaches can be compared in Figs. 11 and 12. The results of the scanning are indicated with circles, whereas the results of the numerical integration are displayed as lines. The accuracy of both approaches is similar, but the numerical integration provides a better resolution while being computationally less expensive.

Displaying the borders of the basins of attractions provides a better understanding of the system's behaviour at PR. At the centre frequency $\Omega_{\mathrm{PE}} = 272560\,\mathrm{s}^{-1}$ ($\Delta\Omega = 0$) of the first PR only one node $[1.54, 58.65]$ exists which is the bifurcated stable limit cycle (see Fig. 11a). Two saddle points $[0.79, 0]$ and $[2.36, 0]$ are visible. They represent the destabilised rest position. For a PE frequency larger than the second bifurcation point $\Delta\Omega = 3853\,\mathrm{s}^{-1}$ the rest position is stable. The rest position appears as a line instead of a point because the phase shift is arbitrary for the steady state. Besides the rest position two to three further attractors are visible in the ranges of the phase space displayed here. In Fig. 11b two non-trivial attractors can be registered: the saddle point $[0.01, 51.28]$ and the node $[1.53, 83.98]$. In Fig. 11c these two attractors come closer to each other in terms

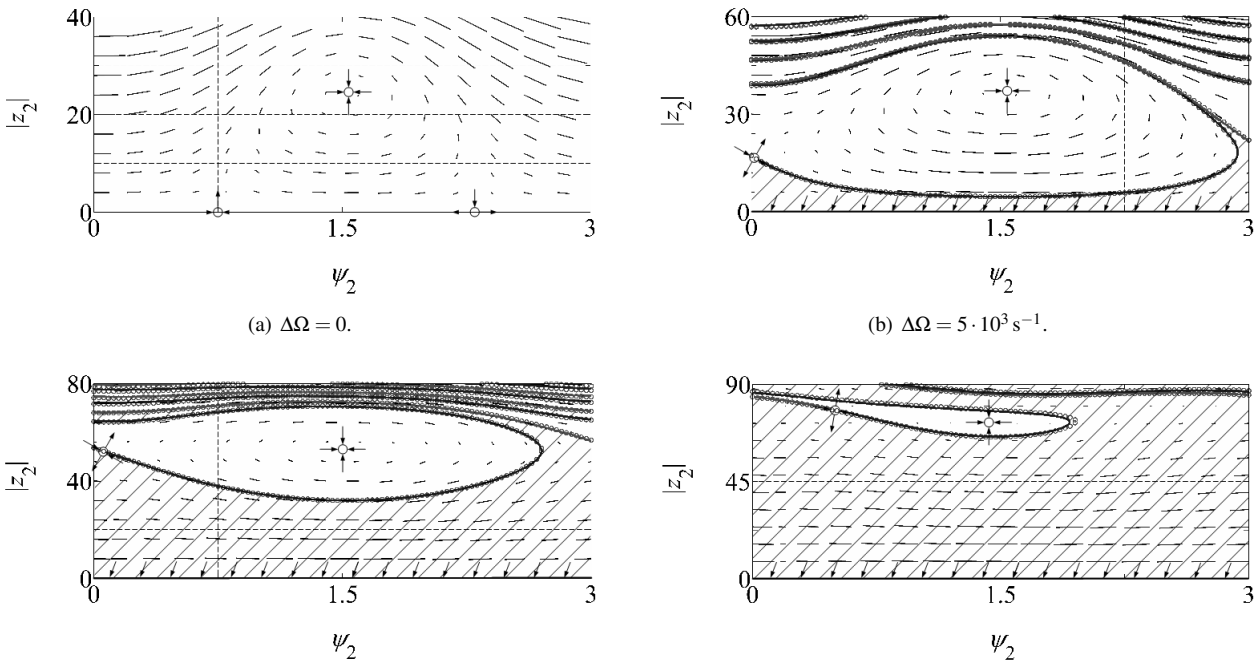

(a) $\Delta\Omega = 0$.

(b) $\Delta\Omega = 5 \cdot 10^3\,\mathrm{s}^{-1}$.

(c) $\Delta\Omega = 15 \cdot 10^3\,\mathrm{s}^{-1}$.

(d) $\Delta\Omega = 30 \cdot 10^3\,\mathrm{s}^{-1}$.

FIGURE 12. POINCARÉ MAPS AT THE PR $\Omega_{\mathrm{PR},2} = 2\omega_2$. HATCHED: BASIN OF ATTRACTION OF THE REST POSITION.

of the phase shift: the saddle point is located at $[0.44, 118.54]$ and the node at $[1.52, 94.28]$. Indeed, another node exists for $\Delta\Omega \geq 4864\,\mathrm{s}^{-1}$. It is not displayed in Fig. 11c and d because it is out of range. Its location is $[3.13, 195.42]$. On the border of its basin of attraction the saddle point $[2.73, 122.84]$ can be identified. Increasing the PE frequency (see Fig. 11d), the three displayed attractors approach each other. For $\Delta\Omega = 8 \cdot 10^3\,\mathrm{s}^{-1}$ the saddle points lie at $[0.73, 119.23]$ and $[2.44, 122.54]$, the node lies at $[1.51, 103.67]$. Further increasing the PE frequency, this node disappears leaving the other node and the rest position as stable attractors.

By analogy, at the centre frequency $\Omega_{\mathrm{PE}} = 442180\,\mathrm{s}^{-1}$ ($\Delta\Omega = 0$) of the second PR only one node $[1.53, 24.42]$ exists which is the bifurcated stable limit cycle (see Fig. 12a). Same as for the first PR the rest position is represented by the two saddle points $[0.79, 0]$ and $[2.36, 0]$. For a PE frequency larger than the second bifurcation point $\Delta\Omega = 3923\,\mathrm{s}^{-1}$ the rest position is stable and appears as a line. In contrast to the first PR, besides the rest position only two further attractors are visible in the ranges of the phase space displayed here. In Fig. 12b two non-trivial attractors can be registered: the saddle point $[0.04, 16.11]$ and the node $[1.52, 36.88]$. In Fig. 12c these two attractors come closer to each other in terms of the amplitude: the saddle point is located at $[0.06, 52.06]$ and the node at $[1.50, 54.02]$. Increasing the PE frequency (see Fig. 12d), the two displayed attractors approach each other. For $\Delta\Omega = 30 \cdot 10^3\,\mathrm{s}^{-1}$ the saddle point lies at $[0.48, 78.09]$ and the node at $[1.37, 73.20]$. Further increasing the PE frequency, this node disappears causing a small interval of the PE Frequency where only the rest position represents a stable attractor.

The basins of attraction are presented in the quasi-modally reduced phase spaces. This presentation already yields all necessary information. A transformation to the physical state variables could be done by Eq. (8): at the first PR $z_1 = 1 \Rightarrow x_1 = 32.524\,\mathrm{nm} \wedge x_2 = 59.745\,\mathrm{nm}$, at the second PR $z_2 = 1 \Rightarrow x_1 = 84.492\,\mathrm{nm} \wedge x_2 = -22.998\,\mathrm{nm}$. However, the main purpose of the Poincaé maps here is to display which state is stable and to compare the power of these states in terms of being able to attract the solution of the system's equation of motion. They enable to check whether the trivial solution is able to attract this solution starting with a certain disturbance at PE frequencies where it is not desired that a bifurcated limit cycle attracts the solution.

CONCLUSION

When investigating non-linear multi degree of freedom PE systems researchers are confronted with numerous challenges compared to conventional systems. The problem of investigating such a system's behaviour and displaying the results, both in meaningfully reduced phase spaces, is addressed here. Quasi-

modally reducing the phase space, the results of a bifurcation analysis for a 2DOF non-linear PE system at PRs can be presented in three dimensional parameter phase spaces. Sections of these parameter phase spaces function as Poincaré maps in which basins of attraction can be displayed.

It is demonstrated how to numerically investigate a rather complicated system time-efficiently and how to present the results in an easy comprehensible way.

ACKNOWLEDGMENT

The research efforts leading to the presented results were supported by a One-year Grant for Doctoral Candidates by the German Academic Exchange Service (DAAD) and a Marietta Blau Grant by the Austrian Ministry of Science, Research and Economy (BMWFW) for the lead author.

REFERENCES

[1] Kniffka, T. J., and Ecker, H., 2015. "Parametrically Excited Microelectromechanical Systems (MEMS)". *e & i Elektrotechnik und Informationstechnik,* ***132***(8), pp. 456–461.

[2] Rhoads, J. F., Shaw, S. W., Turner, K. L., and Baskaran, R., 2005. "Tunable Microelectromechanical Filters that Exploit Parametric Resonance". *Journal of Vibration and Acoustics,* ***127***(5), pp. 423–430.

[3] Jia, Y., Yan, J., Soga, K., and Seshia, A. A., 2013. "Parametrically Excited MEMS Vibration Energy Harvesters with Design Approaches to Overcome the Initiation Threshold Amplitude". *Journal of Micromechanics and Microengineering,* ***23***. 114007.

[4] Welte, J., Kniffka, T. J., and Ecker, H., 2013. "Parametric Excitation in a Two Degree of Freedom MEMS System". *Shock and Vibration,* ***20***(6), pp. 1113–1124.

[5] Kniffka, T. J., 2016. "Numerical, Semi-analytical and Analytical Approaches for Investigating Parametrically Excited Non-linear Systems". PhD Thesis, TU Wien, Vienna, AT.

[6] Zhang, W., Baskaran, R., and Turner, K. L., 2002. "Effect of Cubic Nonlinearity on Auto-parametrically Amplified Resonant MEMS Mass Sensor". *Sensors and Actuators A: Physical,* ***102***(1), pp. 139–150.

[7] Govaerts, W., Kuznetsov, Y. A., and Dhooge, A., 2005. "Numerical Continuation of Bifurcations of Limit Cycles in MATLAB". *SIAM Journal on Scientific Computing,* ***27***(1), pp. 231–252.

[8] Thomas, O., Lazarus, A., and Touzé, C., 2010. "A Harmonic-based Method for Computing the Stability of Periodic Oscillations of Non-linear Structural Systems". In Proc. ASME 2010 IDETC/CIE. DETC2010-28407.

[9] Verhulst, F., 1996. *Nonlinear Differential Equations and Dynamical Systems*. 2nd ed. Springer, Berlin.

[10] Kniffka, T. J., and Ecker, H., 2013. "Observations Regarding Numerical Results Obtained by the Floquet-Method". In Proc. ASME 2013 IDETC/CIE. DETC2013/MSNDC-13292.

[11] Tondl, A., 1998. "To the Problem of Quenching Self-excited Vibrations". *Acta Technica CSAV,* ***43***, pp. 109–116.

[12] Ecker, H., and Pumhössel, T. "Vibration Suppression and Energy Transfer by Parametric Excitation in Drive Systems". In Journal of Mechanical Engineering Science. Proc. Institution of Mechanical Engineers, Part C **226**(8), pp. 2000–2014.

[13] Kniffka, T. J., Welte, J., and Ecker, H., 2012. "Stability Analysis of a Time-periodic 2-dof MEMS Structure". In AIP Conf. Proc. **1493**(559), pp. 559–566.

[14] Kuznetsov, Y. A., 1998. *Elements of Applied Bifurcation Theory*. 2nd ed., Applied Mathematical Sciences **112**. Springer, New York.